Plasmonics
DOI 10.1007/s11468-016-0352-9

Electromagnetically Induced Transparency and Refractive Index Sensing for a Plasmonic Waveguide with a Stub Coupled Ring Resonator

Z. D. Zhang [1,2] · R. B. Wang [1,2,3] · Z. Y Zhang [4] · J. Tang [1,2] · W. D. Zhang [1,2] · C. Y. Xue [1,2] · S. B. Yan [1,2]

Received: 31 March 2016 / Accepted: 1 August 2016

Abstract A plasmonic refractive index sensor based on electromagnetically induced transparency (EIT) composed of a metal-insulator-metal (MIM) waveguide with stub resonators and a ring resonator is presented. The transmission properties and the refractive index sensitivity are numerically studied with the finite element method (FEM). The results revealed an EIT-like transmission spectrum with an asymmetric line profile and a refractive index sensitivity of 1057 nm/RIU are obtained. The coupled mode theory (CMT) based on transmission line theory is adopted to illustrate the EIT-like phenomenon. Multiple EIT-like peaks are observed in the transmission spectrum of the derived structures based on the MIM waveguide with stub resonator coupled ring resonator. To analyze the multiple EIT-like modes of the derived structures, the H_z field distribution is calculated. In addition, the effect of the structural parameters on the EIT-like effect is also studied. These results provide a new method for the dynamic control of light in the nanoscale.

✉ Z. D. Zhang
zdzhang@nuc.edu.cn

S. B. Yan
shubin_yan@nuc.edu.cn

[1] Science and Technology on Electronic Test & Measurement Laboratory, North University of China, Taiyuan 030051, China

[2] Key Laboratory of Instrumentation Science & Dynamic Measurement, Ministry of Eduction, North University of China, Taiyuan 030051, China

[3] School of Mechatronics engineering North University of China, Taiyuan 030051, China

[4] School of Physics and Information Technology, Shaanxi Normal University, Xi'an 710062, China

Keywords Surface plasmon polaritons · Metal-insulator-metal waveguide · Refractive index sensor · Finite element method

Introduction

Surface plasmon polaritons (SPPs) are charge density waves, which are formed by interactions between incident photons and free electrons on metal surfaces [1]. SPPs decay exponentially away from the metal-dielectric interface, which makes it possible for SPPs to overcome the diffraction limit [2, 3]. Metal-insulator-metal (MIM) waveguides are one type of simple SPP waveguides that have the advantages of excellent localized properties, applicable propagation length, and ease of integration [4, 5]. As such, SPPs are very promising for use in highly integrated, nanoscale optical devices [4, 5]. Numerous devices based on MIM waveguides have been demonstrated such as filters [6], all-optical switches [7], plasmonic waveguide modulators [8], plasmonic sensors [9], and demultiplexers [10, 11].

Recently, high sensitivity plasmonic sensors based on MIM waveguide-coupled resonators have attracted interest from researchers [12, 13]. Many studies have focused on designing high sensitivity sensors based on the special optical effects in MIM waveguide-coupled resonators [14], such as electromagnetically induced transparency (EIT)-like and Fano resonance [15, 16]. Fano resonance can also be essentially regarded as the classical analog to EIT in certain conditions [17]. As a quantum interference phenomenon [18, 19], EIT is extremely sensitive to change in the refractive index. Therefore, the EIT-like effect is very promising using the ultra-high sensitivity plasmonic sensors. Chang et al. [20] proposed an infrared plasmonic refractive index nanosensor based on the EIT-like spectral response of waveguide-

Published online: 15 August 2016

coupled resonator systems. The sensitivity, full width at half-maximum, and figure of merit of a plasmonic nanosensor are 733 nm/RIU, 24.11 nm, and 695, respectively. The EIT-like spectral response can be found in many waveguide-coupled resonator systems, such as coupled stub resonator [21], and coupled resonator systems [22]. Therefore, it is possible that combining the EIT-like effect with plasmonic structures would make ultra-high sensitivity plasmonic sensors.

In this paper, we design a plasmonic refractive index nanosensor based on MIM waveguides with a stub resonator coupled ring resonator. The transmission spectrum and magnetic field H_z distributions are simulated using the finite element method (FEM) with a perfectly matched layer (PML) absorbing boundary condition. The coupled mode theory (CMT) [23–25] based on transmission line theory is adopted to illustrate the EIT-like phenomenon. The effect of the structural parameters of the MIM waveguide with stub coupled ring resonator on the propagating properties is studied, and the refractive index sensitivity based on the EIT-like effect is calculated. In addition, the transmission properties of the derived structures based on the MIM waveguide with a stub coupled ring resonator are also investigated.

Structure Model and Analytical Method

Figure 1(a) shows the basic scheme of a plasmonic MIM waveguide-coupled resonator system, which is composed of a MIM waveguide with a stub resonator and a ring resonator. This system is a two-dimensional model, and the gray and white areas represent the Ag (ε_m) and dielectric (ε_d), respectively. The width of the MIM waveguide, stub resonator, and ring resonator is fixed at w = 50 nm to ensure that only the fundamental transverse magnetic (TM_0) mode is supported [16, 26]. g is the coupling distance between the stub resonator and the ring resonator. h_1 is the height of the stub resonator. The inner and outer radii of the ring resonator are r_1 and r_2, respectively. The center radius $R_1$of the ring is the average value of the inner and outer radii, $R_1 = (r_1 + r_2)/2$, as depicted by the dashed circle in Fig. 1. Due to the etching precision

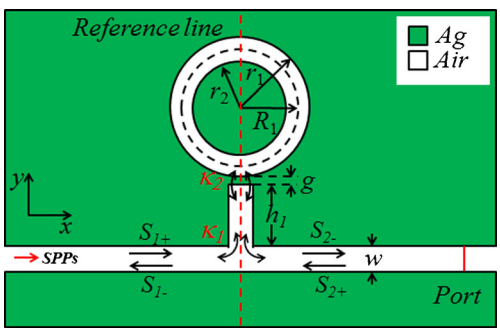

Fig. 1 Schematic for the MIM waveguide with stub coupled ring resonator

only reach to 8 nm at the present time, the difficulty of fabricating this MIM waveguide-coupled resonator system on the control of coupling distance g. However, it is expected to achieve by nano-manufacturing technology in the future. So my studies will provide a theoretical prediction for experimental studies in the future.

The finite element method (FEM) is utilized to analyze the transmission properties of the proposed MIM waveguide-coupled resonator. PMLs are set at the up and bottom boundaries of the structure. The input port (numerical port) and output port are set at the right end and the left end of the MIM waveguide. The permittivity of Ag obeys the Debye-Drude dispersion mode [27] as follows:

$$\varepsilon(\omega) = \varepsilon_\infty + (\varepsilon_s - \varepsilon_\infty) \Big/ (1 + i\omega\tau) + \sigma \Big/ i\omega\varepsilon_0 \tag{1}$$

Here ε_∞ = 3.8344 is the infinite frequency permittivity, ε_s = −9530.5 is the static permittivity, $\sigma = 1.1486 \times 10^7$ S/m is the conductivity, and $\tau = 7.35 \times 10^{-15}$. s is the relaxation time. The TM mode equation [3, 28] for a MIM waveguide is as follows:

$$\tanh(\mathrm{kw}) = -2\mathrm{kp}\alpha_c \Big/ \left(k^2 + p^2\alpha_c{}^2\right) \tag{2}$$

where k is the wave vector in the MIM waveguide. In Equation (2), $p = \varepsilon_d/\varepsilon_m$ and $\alpha_c = [k_0{}^2(\varepsilon_d\text{-}\varepsilon_m) + k^2]^{1/2}$, where ε_d and ε_m are the permittivity of the insulator and metal, respectively. k can be determined by Eq. (2). Thus, the real part of the effective index Re(*neff*) of a MIM waveguide can be expressed as $\mathrm{Re}(neff) = [\varepsilon_m + (k/k_0)^2]^{1/2}$. The effective wavelength $\lambda_{spp} = \lambda_0/\mathrm{Re}(neff)$. The transmittance T is defined as the ratio ($P_{with}/P_{without}$) of the SPP power flows (obtained by integrating the Poynting vector over the channel cross section) of the detecting port with structures (P_{with}) (stub and ring resonator) to without structures ($P_{without}$) [16, 29].

For a MIM waveguide coupling resonator, the resonance wavelength can be determined by the standing wave theory [10, 30].

$$\lambda_m = \frac{2\mathrm{Re}(n_{eff})L}{m - \psi_r/\pi} (m = 1, 2, \cdots) \tag{3}$$

where L is the length of the cavity, positive integer m is the number of antinodes of the standing SPP wave, and ψ_r is the phase shift of the beam reflected at one end of the cavity.

In this part, the CMT is adopted to illustrate the EIT-like phenomenon [23, 24]. The SPPs from the stub directly coupled to MIM waveguide can be treated as an oscillator. k_0 is the decay rate of internal loss in the cavity and it is neglected in this case. k_1 is the coupling coefficient between them. The coupling coefficient between the ring resonator and the stub resonator is denoted by k_2. The amplitude of the incoming and outgoing waves into the cavity is denoted by

S_{i+} and S_{i-} (i = 1 or 2), respectively. When the SPPs are launched into the system from the input port of the MIM waveguide, i.e. $S_{2+} = 0$, the time evolution of the normalized amplitude A_s of the stub and A_{R1} of ring resonator can be expressed [25] as follows:

$$\frac{dA_s}{dt} = (j\omega_s - \kappa_1 - \kappa_2 - \kappa_0)A_s + j\sqrt{\kappa_1}(S_{1+} + S_{2+}) + j\sqrt{\kappa_2}A_{R_1} \quad (4)$$

$$\frac{dA_{R_1}}{dt} = (j\omega_{R_1} - \kappa_2 - \kappa_0)A_{R_1} + j\sqrt{\kappa_2}A_s \quad (5)$$

Here, ω_s and ω_{R1} are the resonance frequency of the stub and the ring resonator, respectively. j is the imaginary unit ($j^2 = -1$). The stub and the ring resonator possess mirror symmetry with respect to the reference line. According to energy conservation, the amplitude of the incoming and the outgoing waves in coupled waveguides should satisfy the following relationships:

$$S_{2-} = S_{1+} + j\sqrt{\kappa_1}A_s \quad (6)$$

$$S_{1-} = S_{2+} + j\sqrt{\kappa_1}A_s \quad (7)$$

Transmission Properties and Theoretical Analysis of the Propose Structure

The transmission spectra of the MIM waveguide with a coupled stub resonator and uncoupled ring resonator are shown in Fig. 2. We found that the transmission spectrum exhibited a resonator dip at $\lambda = 1.225$ μm ($h_1 = 200$ nm), when the ring resonator is removed. A narrow transmission resonance peak with an asymmetric line-shape of the MIM waveguide with a stub coupled ring resonator is formed in the broad stop-band of the MIM waveguide with the stub resonator. This phenomenon is regarded as a typical EIT-like effect, which is derived from special coherent SPPs of constructive and destructive interference between the two optical pathways [31, 32], that is, the resonant mode in the stub is directly excited by the incident wave and the resonance mode in the ring resonator is excited by coupling SPPs. In other words, the broad resonant mode of the stub resonator can be split into two resonant modes, one of which is blue shifted while the other is red shifted, which can be clearly seen in the transmission spectra in Fig. 2.

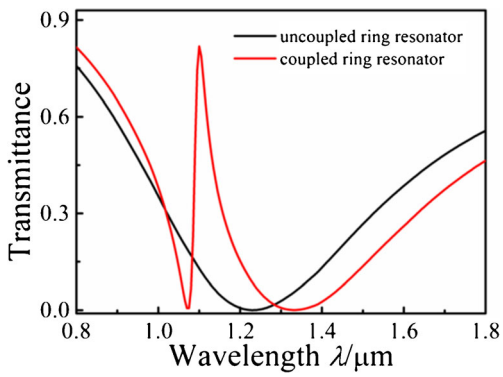

Fig. 2 Transmission spectra of the MIM waveguide only with stub resonator (*black curve*) and with stub coupled ring resonator (*red curve*) for $R_1 = 125$ nm, $h_1 = 200$ nm, and $g = 10$ nm

The H_z field distributions show that there is anti-phase between the stub resonator and MIM waveguide in the MIM waveguide with only a stub resonator at $\lambda = 1.225$ μm (Fig. 3a) and the MIM waveguide with a stub coupled ring resonator at $\lambda = 1.07$ μm (Fig. 3b) and $\lambda = 1.33$ μm (Fig. 3d), respectively. Nevertheless, the H_z field distribution shows that there is in-phase between the directly coupled stub resonator and MIM waveguides at 1.1 μm (Fig. 3c). For $\lambda = 1.225$ μm, the H_z field is very strong in the stub resonator because the SPPs are reflected in the stub resonator. The stub resonator can be regarded as a FP cavity. According to Eq. (2), the dip ($\lambda = 1.225$ μm) corresponds to an effective SPP wavelength of $\lambda_{spp} = 0.878$ μm, so $2h_1/\lambda_{spp} \approx 0.5$, which agrees well with the numerical results shown in Fig. 3a. For $\lambda = 1.07$ μm, a strong H_z field appeared in the stub resonator and ring resonator (as shown in Fig. 3b). The SPPs are limited in the stub resonator and ring resonator due to the destructive interference between the two excitation pathways. One is a broad resonance spectrum from the stub resonator, and the other is a narrow resonance spectrum resulting from the ring resonator. Therefore, the SPPs do not propagate to the other end of the MIM waveguide. For the EIT-like peak ($\lambda = 1.1$ μm), the SPPs do not resonate in the stub resonator (as shown in Fig. 3c). It means that incident SPPs and the SPPs escaping from the stub resonator into the MIM waveguide generate a coherence enhancement. For $\lambda = 1.33$ μm, the strong H_z field occurs in the stub resonator, but few H_z field distributions

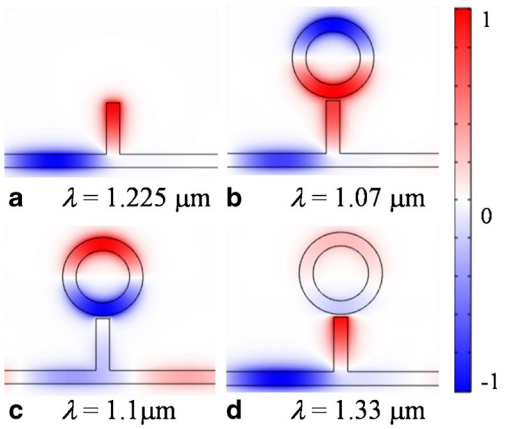

Fig. 3 Contour profiles of the normalized H_z field distributions of the MIM waveguide with a stub-shape resonator: **a** $\lambda = 1.225$ μm; the contour profiles of the normalized H_z field distributions of the MIM waveguide with a stub-shape coupled ring resonator: **b** $\lambda = 1.07$ μm, **c** $\lambda = 1.1$ μm, and **d** $\lambda = 1.33$ μm

occur in the ring resonator (see Fig. 3d) because the $\lambda = 1.33$ μm is far from the resonant mode ($\lambda = 1.1$ μm) of the ring resonator. Namely, the conditions of interference destructive of the SPPs are not satisfied, and then the SPP transmission is inhibited.

The transmittance T of the MIM waveguide with stub coupled ring resonator system can be solved by Eqs. (4)–(6) to illustrate in detail the EIT-like phenomenon. T is as follows:

$$T = \left|\frac{S_{2-}}{S_{1+}}\right|^2 = \left|\frac{j(\omega-\omega_s) + \kappa_2 + \frac{\kappa_2}{j(\omega-\omega_{R_1})+\kappa_2}}{j(\omega-\omega_s) + (\kappa_1+\kappa_2) + \frac{\kappa_2}{j(\omega-\omega_{R_1})+\kappa_2}}\right|^2 \quad (8)$$

From Eq. (8), when the stub resonator uncoupled ring resonator, the transmittance T can be expressed as:

$$T = \left|\frac{S_{2-}}{S_{1+}}\right|^2 = \left|\frac{j(\omega-\omega_s)}{j(\omega-\omega_s) + \kappa_1}\right|^2 \quad (9)$$

Namely, the wave (ω_s) will be suppressed and not transmitted in the MIM waveguide system when $\omega_s = \omega$ in the MIM waveguide with a stub resonator.

A ring resonator R_1 is added into the MIM waveguide with stub resonator system; the transmittance $T = |(\kappa_2 + 1)/(\kappa + \kappa_2 + 1)|^2$ when $\omega_{R1} = \omega_s = \omega$, which means an EIT-like peak is emerging.

In addition, Eq. (8) also indicates that there EIT-like peak emerged at frequency $\omega_s = \omega$ as long as the ω_s and ω_{R1} are close to each other, and the corresponding transmittance can be determined as:

$$T = \left|\frac{j(\omega_{R_1}-\omega_s) + \kappa_2 + 1}{j(\omega_{R_1}-\omega_s) + (\kappa_1+\kappa_2) + 1}\right|^2 \quad (10)$$

The Influence of the Structural Parameters on the Transmission Properties

According to the simulation results, we find that the transmission spectrum of the plasmonic waveguide system can be tuned through the change in the structure parameters. First, we calculated the transmission spectra for different radii of the ring resonator (R_1) with $h_1 = 200$ nm and $g = 10$ nm, and the transmission spectra of $R_1 = 115$, 120, 125, 130, 135 nm are displayed in Fig. 4a, respectively. With decreasing R_1, the EIT-like peak shifts blue. Successively, the influence of the stub resonator height h_1 on the EIT-like peak is investigated when $R_1 = 125$ nm and $g = 10$ nm. As shown in Fig. 4b, the position of the EIT-like peak is almost unaffected by increasing h_1, but the band width increase with increasing h_1. Furthermore, the transmission spectra for different coupling distances (g) between the stub resonator and ring resonator with $h_1 = 200$ nm and $R_1 = 125$ nm are calculated. The transmission spectra of $g = 6$, 8, 10, 12 nm are shown in Fig. 4c. With the increase of g, the bandwidth of the EIT-like peak becomes smaller. In addition, the refractive index sensitivity based on the EIT-like effect is investigated by filling different refractive index ($n = 1.0$, 1.33, 1.34, and 1.35) dielectrics into the resonators. The other structural parameters are set as $h_1 = 200$ nm and $R_1 = 125$ nm. With increasing n, the EIT-like peak exhibits a red shift (as shown in Fig. 4d). The proposed structures can be used as high sensitivity nanosensors with the sensitivity of 1057 nm/RIU (per unit variations of the refractive index). We find that the R_1 and the refractive index n increase induce the EIT-like peak red shift, which agree well with the Eq. (3). That is, the λ_m increase with the increase of L and the Re(n_{eff}) according to the Eq. (3). In conclusion, we can easily manipulate the EIT-like behavior by modifying the radius R_1 in the ring resonator, the height h_1 of the stub resonator, and the coupling distance g between the stub resonator and the ring resonator.

Transmission Properties of the Derivative Structure

Multiple EIT Induced by Adding a Stub Resonator

A double EIT-like peak can be observed in the transmission spectra of the asymmetric derivative structure by adding another stub resonator (the height h_2) at the stub resonator opposite of the structure (in Fig. 1), and the asymmetric derivative structure is shown in Fig. 5a. The transmission spectrum of the derivative structure with $R_1 = 125$ nm and $h_1 = h_2 = 200$ nm is shown in Fig. 5b. Compared to the transmission spectrum (Fig. 2) of the MIM waveguide with a single stub coupled ring resonator, the EIT-like peak ($\lambda = 1.09$ μm) still occur in the transmission spectrum, but another new EIT-like peak ($\lambda = 1.34$ μm) was observed in the transmission spectrum (as shown in Fig. 5b). The corresponding H_z field distributions for $\lambda = 1.09$ μm are shown in the left inset in Fig. 5b. We find that the H_z field distribution (left inset) in Fig. 5b was same as that shown in Fig. 3c. Therefore, they have similar SPP propagation behaviors in the upper stub resonator and ring resonator. This can be explained by the above analysis. For $\lambda = 1.34$ μm, we find that a strong H_z field mainly occur in the upper stub resonator and down stub resonator, but a very weak H_z field occur in the ring resonator (as shown in the right inset in Fig. 5(b)). The SPPs show a Fabry-Perot-resonator-like behavior in the derivative structure. According to Eq. (1), the effective SPP wavelength of the EIT-like peaks ($\lambda = 1.09$ μm and $\lambda = 1.34$ μm) was $\lambda_{spp} = 0.779$ μm and 0.962 μm. At $\lambda = 1.09$ μm, $2\pi R_1/$

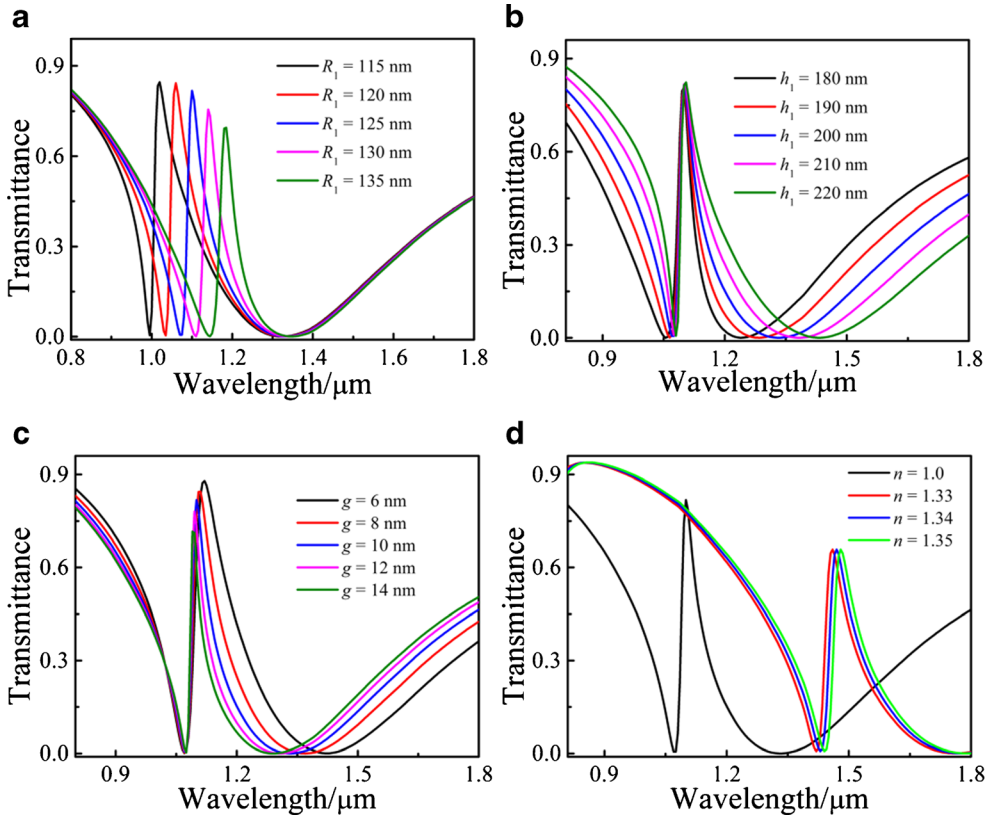

Fig. 4 **a** Transmission spectra for different radii R_1 of the ring resonator with h_1 = 200 nm, g = 10 nm, and n = 1. **b** Transmission spectra for different heights h_1 of the upper stub resonator with R_1 = 125 nm, g = 10 nm, and n = 1. **c** Transmission spectra for different coupling distances between the stub resonator and ring resonator with R_1 = 125 nm, h_1 = 200 nm, and n = 1. **d** Transmission spectra for different filling dielectric refractive indexes n with R_1 = 125 nm, h_1 = 200 nm, and g = 10 nm

$\lambda_{spp} \approx 1$ for ring resonator and $2(h_1 + h_2 + w)/\lambda_{spp} \approx 1.2$ for upper and down stub resonator. The $\lambda_{spp} = 0.779$ μm does not meet the wave resonance condition of the upper and down stub resonator, but it meets the ring resonator condition. As shown in the inset of Fig. 5b, the H_z field distributions agrees well with the numerical results. But at λ = 1.34 μm, $2\pi R_1/\lambda_{spp} \approx 0.82$ for ring resonator and $2(h_1 + h_2 + w)/\lambda_{spp} \approx 0.94$ for upper and down stub resonator. The SPPs ($\lambda_{spp} = 0.962$ μm) only meet the wave resonance condition of the upper and down stub resonator but do not meet the ring resonator condition. Therefore, SPPs can resonate between the upper and lower stub resonators but cannot resonate in the ring resonator. In addition, the transmission spectra of h_2 = 200, 225, 250, 275, and 300 nm are displayed in Fig. 5c. With the increase of h_2, the EIT-like peak

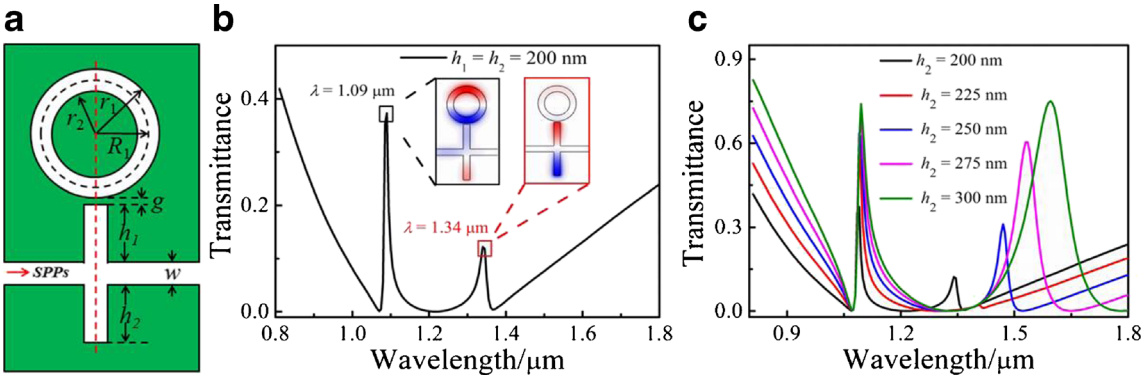

Fig. 5 **a** Schematic for the asymmetry derivate structure. **b** Transmission spectrum of the asymmetry derivate structure with R_1 = 125 nm, h_1 = 200 nm, and h_2 = 200 nm; the *left inset* and the *right inset* are the normalized H_z field distributions at λ = 1.09 μm and at λ = 1.34 μm. **c** Transmission spectra for different heights of the down stub resonator with R_1 = 125 nm and h_1 = 200 nm

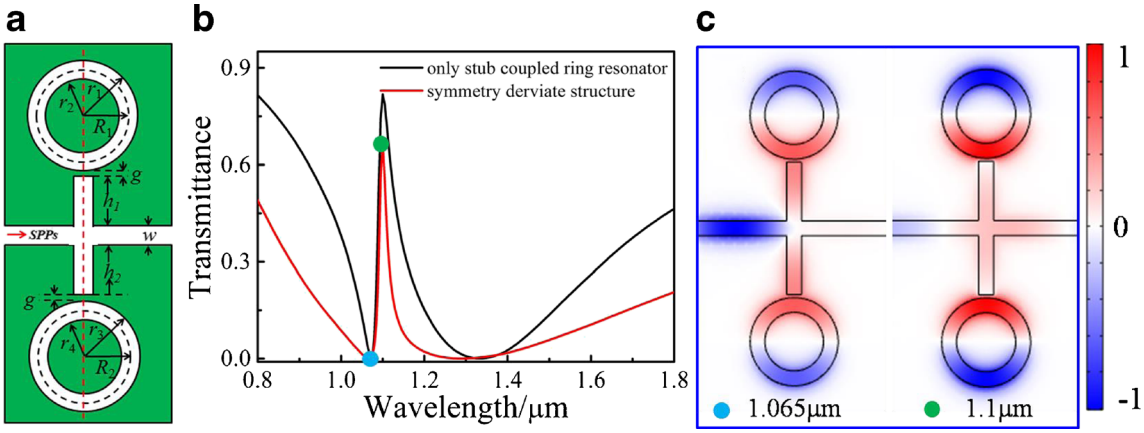

Fig. 6 **a** Schematic for the symmetry derivative structure. **b** Transmission spectrum (*black line*) for MIM waveguide with only stub coupled ring resonator and transmission spectrum (*red line*) for the symmetry derivative structure with $R_1 = R_2 = 125$ nm, $h_1 = h_2 = 200$ nm. **c** The H_z field distribution for the symmetry derivate structure at $\lambda = 1.065$ and $\lambda = 1.1$ μm

with $\lambda = 1.09$ μm do not shift, but EIT-like peaks at longer wavelength range red shift. This implies that the former is mainly dependent on R_1, but the latter is mainly determined by h_1 and h_2.

EIT-Like Effect for Two Coupled Pair of the Stub Resonator and Ring Resonator

In this section, the transmission properties and H_z field distribution of the symmetric derivative structure are investigated. The structure schematics are shown in Fig. 6a. Two coupled pairs of the stub resonator and ring resonator are symmetric with respect to the MIM waveguide. R_3 is the radius of the down ring resonator. The structural parameters of the derivative structure are set to $h_1 = h_2 = 200$ nm, $R_1 = R_2 = 125$ nm, and $g = 10$ nm. The transmission spectrum (black line) of the MIM waveguide with single stub resonator coupled ring resonator and the transmission spectrum (red line) of the symmetric derivative structure are shown in Fig. 6b. Compared to the MIM waveguide with the single stub coupled ring resonator, the bandwidth of the EIT-like peak for the symmetric derivate structure is much narrower. The H_z field distribution of the symmetric derivate structure at the wavelength incident of the dip ($\lambda = 1.065$ μm) and the peak ($\lambda = 1.1$ μm) are shown in Fig. 6(c).

The transmission properties of an asymmetric derivate structure composed of the MIM waveguide with two asymmetric coupled pair stub resonators and a ring resonator ($h_1 = h_2$ and $R_1 \neq R_2$ or $h_1 \neq h_2$ and $R_1 = R_2$) are investigated. The transmission spectrum of the asymmetric derivate structure with $R_2 = 125$, 175, 200, and 225 nm and fix at $h_1 = h_2 = 200$ nm and $R_1 = 125$ nm are shown in Fig. 7a. For $R_1 = 105$ nm, two EIT-like peaks with asymmetric sharp line profiles are observed in the transmission spectrum, but only one EIT-like peak is seen with $R_1 = 125$ nm. When $R_1 = 145$ nm, two EIT-like peaks are observed in the transmission spectra. Three EIT-like peaks with asymmetric sharp line profiles are observed in the transmission spectrum for $R_1 = 145$ nm in the longer wavelength range. The effect of h_1 on the transmission spectra is investigated by increasing h_1 from $h_1 = 180$ nm to $h_1 = 230$ nm with fix at $R_1 = R_2 = 125$ nm and $h_2 = 200$ nm. The transmission spectra of the asymmetric derivative structure with $h_1 = 180$, 190, 200, 210, 220, and 230 nm are shown in Fig. 7b. As increasing h_1, the EIT-like peak ($\lambda = 1.1$ μm) does not shift, but the EIT-like peaks at longer wavelengths ($\lambda > 1.3$ μm) shift red.

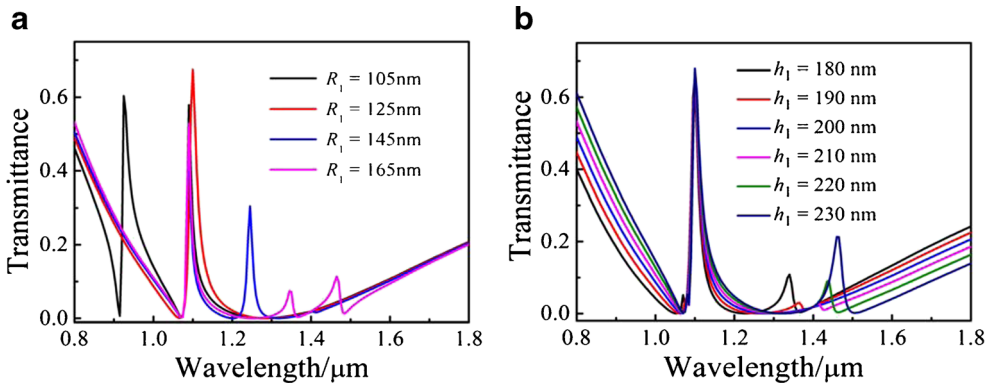

Fig. 7 (a) Transmission spectra for different radii of the upper ring resonator with $h_1 = h_2 = 200$ nm and $R_2 = 125$ nm. **b** Transmission for different heights of the upper sub resonator with $R_1 = R_2 = 125$ nm and $h_2 = 200$ nm

Conclusions

In this paper, a MIM waveguide-coupled resonator system, MIM waveguide with a stub coupled ring resonator, is proposed and investigated using the FEM. The simulation results show that the EIT-like effects can be observed and the transparency window peak can be easily controlled by the structural parameters. The EIT-like effect of the MIM waveguide with stub resonator coupled ring resonator is illustrated in detail by the CMT model. Furthermore, the plasmonic refractive index sensitivity based on the EIT-like effects is investigated by filling the dielectrics with different refractive indices into the cavity, and a sensitivity of 1057 RIU/nm was obtained. In addition, multiple EIT-like peaks are observed in the transmission spectra of the asymmetric derivate structure, but one EIT-like peak can be obtained in the transmission spectra of the MIM waveguide with a stub coupled ring resonator and symmetric derivate structure.

Acknowledgments This work was supported by the National Natural Science Foundation of China (Grant Nos. 61275166 and 61575117), the National Science Fund for Distinguished Young Scholars (Grant No. 51225504 and 61525107), the Natural Science Research Foundation of North University of China (Grant No 110246), Open Foundation of Science and Technology on Electronic Test and Measurement Laboratory of North University of China (Grant No. ZDSYSJ2015003), Program for the Top Young and Middle-aged Innovative Talents of Higher Learning Institutions of Shanxi, and the North University of China Science Fund for Distinguished Young Scholars.

References

1. Barnes WL, Dereux A, Ebbesen TW (2003) Surface plasmon subwavelength optics. Nature 424(6950):824–830
2. Han Z, Bozhevolnyi SI (2012) Radiation guiding with surface plasmon polaritons. Rep Prog Phys 76(1):016402
3. Zayats AV, Smolyaninov II, Maradudin AA (2005) Nano-optics of surface plasmon polaritons. Phys Rep 408(3):131–314
4. Zia R, Schuller JA, Chandran A, Brongersma ML (2006) Plasmonics: the next chip-scale technology. Mater Today 9(7):20–27
5. Fang Y, Sun M (2015) Nanoplasmonic waveguides: towards applications in integrated nanophotonic circuits. Light Sci Appl 4(6):e294
6. Zhu JH, Wang QJ, Shum P, Huang XG (2010) A simple nanometeric plasmonic narrow-band filter structure based on metal–insulator–metal waveguide. IEEE T Nanotechnol 10(6):1371–1376
7. Lu H, Liu X, Wang L, Gong YK, Mao D (2011) Ultrafast all-optical switching in nanoplasmonic waveguide with Kerr nonlinear resonator. Opt Express 19(4):2910–2915
8. Piao X, Yu S, Park N (2012) Control of Fano asymmetry in plasmon induced transparency and its application to plasmonic waveguide modulator. Opt Express 20(17):18994–18999
9. Ye J, Van Dorpe P (2011) Improvement of figure of merit for gold nanobar array plasmonic sensors. Plasmonics 6(4):665–671
10. Hu F, Yi H, Zhou Z (2011) Wavelength demultiplexing structure based on arrayed plasmonic slot cavities. Opt Lett 36(8):1500–1502
11. Chen J, Li Z, Li J, Gong QH (2011) Compact and high-resolution plasmonic wavelength demultiplexers based on Fano interference. Opt Express 19(10):9976–9985
12. Chen Z, Wang W, Cui L, Yu L, Duan G, Zhao Y, Xiao J (2014) Spectral splitting based on electromagnetically induced transparency in plasmonic waveguide resonator system. Plasmonics 10(3):721–727
13. Wen K, Hu Y, Chen L, Zhou J, Lei L, Meng Z (2016) Single/dual Fano resonance based on plasmonic metal-dielectric-metal waveguide. Plasmonics 11(1):315–321
14. Lu H, Liu X, Mao D, Wang G (2012) Plasmonic nanosensor based on Fano resonance in waveguide-coupled resonators. Opt Lett 37(18):3780–3782
15. Zhan S, Li H, Cao G, He Z, Li B, Xu H (2014) Theoretical analysis of plasmon-induced transparency in ring-resonators coupled channel drop filter systems. Plasmonics 9(6):1431–1437
16. Zhang ZD, Wang HY, Zhang ZY (2012) Fano resonance in a gear-shaped nanocavity of the metal–insulator–metal waveguide. Plasmonics 8(2):797–801
17. Peng B, Özdemir SK, Chen W, Nori F, Yang L (2014) What is and what is not electromagnetically induced transparency in whispering-gallery microcavities. Nat Commun 5:5082–5092
18. He LY, Wang TJ, Gao YP, Cao C, Wang C (2015) Discerning electromagnetically induced transparency from Autler-Townes splitting in plasmonic waveguide and coupled resonators system. Opt Express 23(18):23817–23826
19. Hu M, Wang F, Liang R, Zhou S, Xiao L (2015) Plasmonic-induced transparency based on plasmonic asymmetric dual side-coupled cavities. Phys Lett A 379(6):581–584
20. Ni B, Chen XY, Xiong DY, Liu H, Hua GH, Chang JH, Zhang JH, Zhou H (2015) Infrared plasmonic refractive index-sensitive nanosensor based on electromagnetically induced transparency of waveguide resonator systems. Opt Quant Electron 47(6):1339–1346
21. Zafar R, Salim M (2014) Wideband slow light achievement in MIM plasmonic waveguide by controlling Fano resonance. Infrared Phys Technol 67(67):25–29
22. Chen J, Wang C, Zhang R, Xiao J (2012) Multiple plasmon-induced transparencies in coupled-resonator systems. Opt Lett 37(24):5133–5135
23. Haus HA (1983) Waves and fields in optoelectronics. Prentice-Hall, New Jersey
24. Haus HA, Huang WP (1991) Coupled-mode theory. Proc IEEE 79(10):1505–1518
25. Lai G, Liang R, Zhang Y, Bian Z, Yi L, Zhan G, Zhao R (2015) Double plasmonic nanodisks design for electromagnetically induced transparency and slow light. Opt Express 23(5):6554–6561
26. Kekatpure RD, Hryciw AC, Barnard ES, Brongersma ML (2009) Solving dielectric and plasmonic waveguide dispersion relations on a pocket calculator. Opt Express 17(26):24112–24129
27. Gai H, Wang J, Tian Q (2007) Modified Debye model parameters of metals applicable for broadband calculations. Appl Opt 46(12):2229–2233
28. Kekatpure RD, Barnard ES, Cai W (2010) Phase-coupled plasmon-induced transparency. Phys Rev Lett 104(24):243902
29. Zhang ZY, Wang JD, Zhao YN, Lu D, Xiong ZH (2011) Numerical investigation of a branch-shaped filter based on metal-insulator-metal waveguide. Plasmonics 6:773–778
30. Xu Q, Sandhu S, Povinelli ML, Shakya J, Fan S, Lipson M (2006) Experimental realization of an on-chip all-optical analogue to electromagnetically induced transparency. Phys Rev Lett 96(12):123901
31. Huang Y, Ma LW, Hou MJ, Zhang ZJ (2016) Universal near-field interference patterns of Fano resonances in two-dimensional plasmonic crystals. Plasmonics. doi:10.1007/s11468-016-0187-4
32. Francescato Y, Giannini V, Maier SA (2012) Plasmonic systems unveiled by Fano resonances. ACS Nano 6(2):1830–1838